Extended Abstracts of the 2018 International Conference on Solid State Devices and Materials, Tokyo, 2018, pp719-720

High Mobility Anisotropic Black Phosphorus Nanoribbons Field-Effect Transistor: Impact of Crystal Orientation, Dimension Scaling and Hydrogen Anneal

Xuewei Feng[1,2], Xin Huang[1,2], Li Chen[1,2], Lin Wang[1,2], and Kah-Wee Ang[1,2,#].

[1]Department of Electrical and Computer Engineering, National University of Singapore, 4 Engineering Drive 3, Singapore 117583

[2]Centre for Advanced 2D Materials, National University of Singapore, 6 Science Drive 2, Singapore 117546

Phone: +65 6516-2575, Fax: +65 6779-1103, [#]Email: eleakw@nus.edu.sg

ABSTRACT

We demonstrate a first-of-its-kind black phosphorus nanoribbons field-effect transistor (BPNR-FET) and systematically investigate methods for enhancing its anisotropic carrier transport. The BPNR-FET shows a strong dependence on crystal orientation where best mobility performance (862 cm^2/Vs) is achieved in armchair-oriented nanoribbons. A downscaling of nanoribbon width is shown to improve the short channel effect due to a better electrostatic control. Furthermore, hydrogenation is employed to effectively passivate the dangling bonds and heal the nanoribbon edge defects, leading to hysteresis and contact resistance improvement in addition to hole mobility enhancement.

INTRODUCTION

Black phosphorus (BP) planar p-FET have ultrahigh hole mobility up to 1000 cm^2/Vs [1]. For BP transistors, most researches are focusing on contact engineering or doping technique to improve hole mobility [2-5]. However, in ultra-scaled devices, three-dimensional architectures such as nanoribbon or FinFET are required to provide excellent electrostatic control to suppress short-channel effects. To date, p-FinFET using Ge, SiGe, or GeSn have been widely investigated beyond silicon [6-8]. 2D materials such as BP, by virtue of its layered structure and in-plane anisotropy properties, is expected to deliver even better performance when integrated with 3D structure as compared to bulk planar technology. However, no work has been done to realize nanoribbon-based BP field-effect transistor to date.

Here, for the first time, high performance BPNR-FETs with a high hole mobility of 862 cm^2/Vs is demonstrated. A CMOS-compatible top-down reactive ion etching (RIE) is used to realize large area nanoribbons array down to sub-60 nm. The adoption of 3D device structure effectively reduces the subthreshold swing (*SS*) and improves the current on/off ratio as compared with bulk BP-FET, confirming an enhanced electrostatic gate control over the top- and side-wall channels. Moreover, hydrogen treatment is employed to heal the nanoribbon edge defects, leading to hole mobility improvement from 703 cm^2/Vs to 862 cm^2/Vs along the armchair crystal direction.

DEVICE FABRICATION

BPNR-FET structure and key fabrication steps are shown in **Fig. 1**. The AFM image in **Fig. 2** shows the complete anisotropic BPNR-FET along armchair (AC) and zigzag (ZZ) crystalline orientation. The nanoribbon width in this work, as precisely measured by SEM, is based on 60 nm but smooth 30 nm ribbons are also achieved. After exfoliation onto p+ Si/SiO_2 substrate, polarized Raman spectra of the BP flake under different sample rotation angles were collected (**Fig. 3**). The intensity of A_g^2 mode varies with a period of 180° and maximum intensity is found to be strongest along the armchair direction. The BPNRs-array is realized *via* a CHF_3/O_2 reactive ion etching (RIE) method. A precisely controlled layer-by-layer thinning with an etch rate of 0.6 nm/s is achieved compared with SF_6 and pure CHF_3 plasma. The recipe also achieves a good selectivity of BP over PMMA (1:5) which acts as a soft mask. The cross-section HR-TEM image taken across the BPNRs confirm that the crystallinity of BP nanoribbons is preserved, showing no detrimental effects due to reactive ion etching (**Fig. 4**).

RESULTS AND DISCUSSION

A. Surface Crystallographic Orientation

The transfer characteristic (I_d-V_g) of BPNR-FET along AC and ZZ channel direction is compared in **Fig. 6**. As compared with zigzag direction, the armchair-oriented BPNR-FET achieves a 3.2 times higher maximum current. This signifies the superior hole transport properties along AC channel due to a lighter hole effective mass of 0.15 m_0 than the zigzag direction (1.54 m_0) [9]. The linear output characteristic I_d-V_d in **Fig. 7** confirms the formation of high-quality Ohmic contacts between the metal electrodes and BPNR channel. **Fig. 8** shows the calculated hole field-effect mobility and intrinsic mobility. By decoupling the influence of contact resistance, a high peak intrinsic mobility of 703 cm^2/Vs and 300 cm^2/Vs is achieved along AC and ZZ direction, respectively.

B. Nanoribbons Width and Thickness Scaling

Fig. 9 compares the I_d-V_g curves of bulk BP-FET and BPNR-FET with different nanoribbons width of 200 nm and 60 nm. Clearly, an increased on-state linear current density by nearly an order of magnitude and a reduced *SS* from 2.69 V/dec to 563 mV/dec are achieved when the BP is scaled from bulk to 60 nm wide. The enhanced nanoribbon transistor performance could be attributed to the three-dimensional top- and side-wall electrostatic gate control which effectively improves the short-channel effect. **Fig. 10** plots the non-monotonic variation of the intrinsic hole mobility as a function of channel thickness, where peak mobility is achieved when the BP is 28 nm thick. However, as the BP is scaled below sub-5 nm, the mobility is observed to decrease due to surface roughness scattering at the BP/SiO_2 interface. Nonetheless, a hole mobility of ~145 cm^2/Vs is still maintained in a 4 nm thick device.

C. Hydrogen Thermal Anneal

Fig. 11 and 12 shows the I_d-V_g of the BPNR-FET before and after hydrogen anneal treatment at 200 °C for 20 mins. The hysteresis reduction as shown in **Fig. 13** implies the elimination of charge traps located at the BPNR/high-κ gate dielectric and metal/BP interfaces. This results in a reduction of D_{it} along AC and ZZ directions by 35 % and 69 %, respectively, which confirms the effectiveness of hydrogen in passivating the dangling bonds and healing the defects induced by RIE. By physically sputtering the S/D area and treating the Ni contact with forming gas, the Ni contact resistance has also been significantly reduced to a low value of 1.38 Ω-mm (**Fig. 14**) as compared with previously reported values of 3.15 Ω-mm and 3.73 Ω-mm [4,5]. The larger contact resistance at zigzag-oriented interface implies a higher Schottky barrier height (SBH) due to a stronger Fermi level pinning (FLP) by the interface defects. Apparently, hydrogen anneal could effectively eliminate the FLP effect at the ZZ interface and improve the contact resistance to a value comparable to the AC interface.

D. Mobility Benchmarking

Fig. 15 benchmarks the mobility of the state-of-the-art non-planar field-effect transistors featuring various channel materials. The peak hole mobility of BPNR-FET along AC direction, which is estimated to be 862 cm^2/Vs after hydrogen anneal, is shown to outperform Si nanowire, strained-SiGe, Ge and GeSn FinFET [6-8,12]. Noteworthily, nanoribbon FETs based on TMD materials such as MoS_2 and CdS are showing n-type behavior [10,11]. Although graphene p-FET has a higher mobility, the inherent zero bandgap compromises its off-state leakage current while the synthesis method *via* unwrapping of carbon nanotube is not CMOS-compatible [13]. Further improvement is expected with process optimization such as nanoribbon width scaling and gate stack engineering.

CONCLUSION

A world's first BPNR-FET featuring top metal gate/high-κ gate dielectric is demonstrated with a high hole mobility reaching 862 cm^2/Vs. The adoption of 3D nanoribbon structure effectively improves the control of short channel effect, leading to enhanced transistor performance over bulk BP-FET. The use of hydrogen anneal effectively improves the hysteresis, reduces the contact resistance and simultaneously enhances the hole mobility. This work unravels the superior performance underscore a conceptually new BPNR-FET, paving the way towards the development of non-planar devices based on 2D materials platform.

REFERENCES

[1] Li, L., *et al.*, *Nat. Nanotechnol.* 2014, 9, 372. [2] Tan, W. C., *et al.*, *Adv. Mater.* 2017, 26, 1700503. [3] Saito, Y *et al.*, *ACS Nano* 2015, 9, 3192. [4] Ling, Z.-P. *et al.*, *Sci. Rep.* 2015, 5, 18000. [5] Du, Y. *et al., ACS Nano* 2014, 8, 10035 [6] J Mitard, J. *et al., VLSI,* 2016*,* pp.35. [7] Hashemi, P., *VLSI* 2015, pp.T16 [8] Dian, L. *et al*., *VLSI*, 2017, pp.T198. [9] Han, X. *et al.*, *Nano Lett.* 2014, 14, 4607. [10] Liu, H. *et al.*, *IEEE Electron Device Lett.* 2012, 33, 1273. [11] Duan, X. *et al.*, *Nature* 2003, 425, 274. [12] Hashemi, P., *IEDM* 2010, pp.34-5 [13] Jiao, L. *et al*., *Nat. Nanotechnol.* 2010, 5, 321.

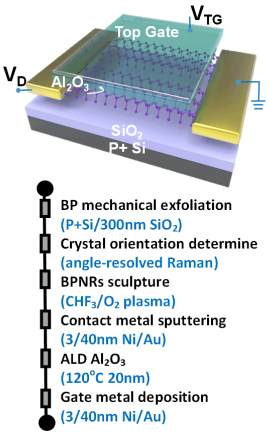

Fig. 1. Schematic diagram and fabrication flow of the BPNR-FET.

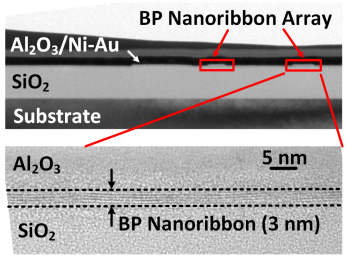

Fig. 4. HR-TEM micrograph shows that the crystallinity of BP nanoribbons is preserved after plasma etching.

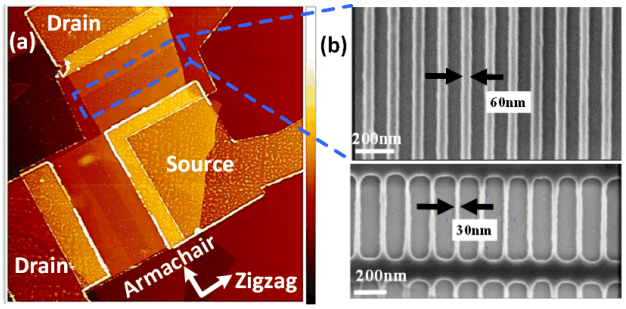

Fig. 2. (a) AFM image showing armchair- and zigzag-oriented BPNR-FET together with S/D and top gate. (b) SEM images of BPNR array with width is 60 nm and 30 nm.

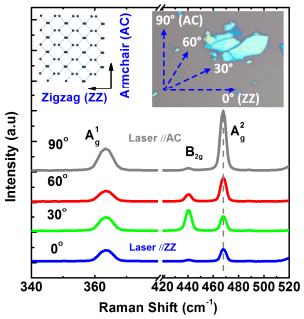

Fig. 3. Angle-resolved Raman spectra. Armchair is along 90° direction where A_g^2 is strongest.

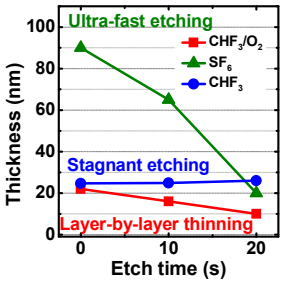

Fig. 5. BP etch rate using different feed gases such as CHF_3/O_2, pure CHF_3 and SF_6. A layer-by-layer thinning of BP (0.6nm/s) is achieved with CHF_3/O_2.

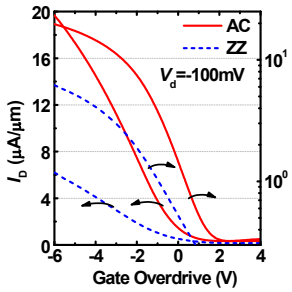

Fig. 6. I_d-V_g Characteristics comparisons of BPNR-FET along armchair (AC) and zigzag (ZZ) crystalline direction. AC is observed to be a more favorable transport channel.

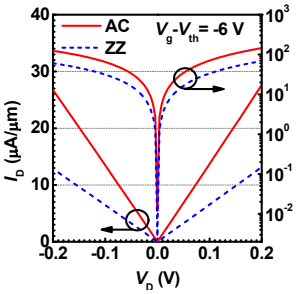

Fig. 7. I_d-V_d output characteristics comparison of the same BPNR-FET along AC and ZZ direction. An Ohmic-contact is formed at strong hole accumulation region when gate overdrive is -6 V.

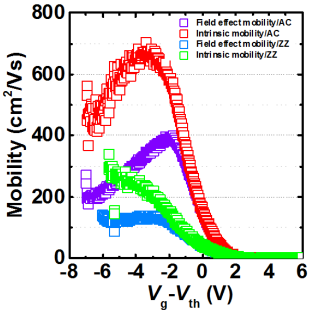

Fig. 8. The field-effect mobility and intrinsic mobility after decoupling the influence of contact resistance along AC and ZZ orientation.

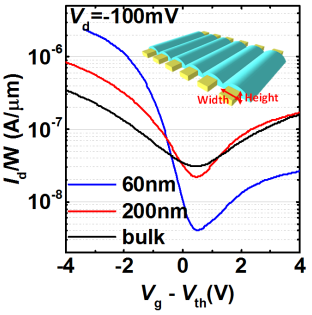

Fig. 9. The I_d-V_g characteristics of bulk BP-FET and BPNR-FET with nanoribbon width of 200 nm and 60 nm.

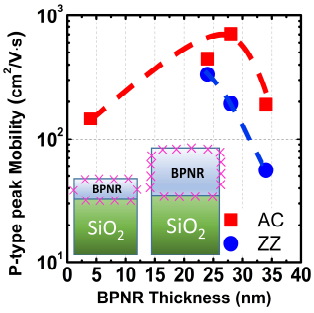

Fig. 10. The p-type intrinsic mobility *vs* BP thickness. The non-monotonic variation of mobility implies different scattering mechanism.

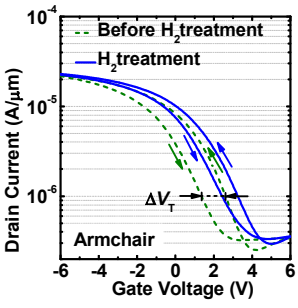

Fig. 11. Transfer characteristic of BPNR-FET with transport channel along armchair direction with and w/o forming gas annealing (FGA).

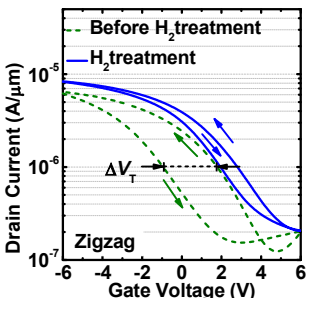

Fig. 12. Transfer characteristic of BPNR-FET with transport channel along zigzag direction with and w/o forming gas annealing (FGA).

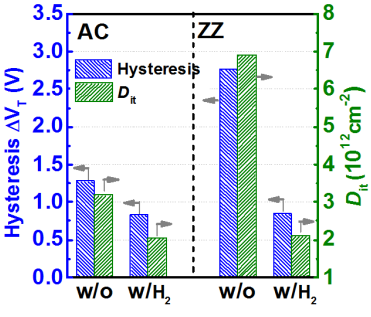

Fig. 13. The Hysteresis and D_{it} comparisons of BPNR-FET along AC and ZZ direction before and after hydrogen anneal treatment.

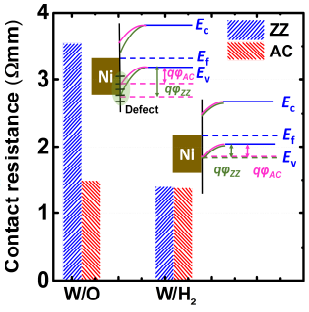

Fig. 14. Hydrogen treatment removes Fermi level pinning effect in zigzag interface and achieves an ultralow contact resistance of 1.38 Ω-mm.

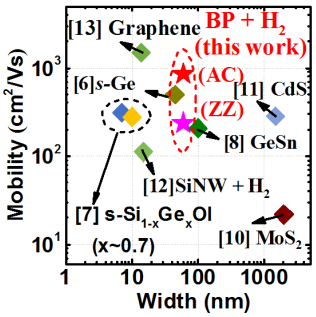

Fig. 15. Benchmarking of mobility for advanced transistor structures. BP stands out among other channel materials, e.g. Ge, GeSn, MoS_2 etc.

Acknowledgement: This research is supported by A*STAR Science and Engineering Research Council Grant (No. 152-70-00013), and by the National Research Foundation, Prime Minister's Office, Singapore under its medium sized center program.